Discrete-element modeling of shock compression of polycrystalline copper

K. Yano and Y. Horie
Department of Civil Engineering, North Carolina State University, Raleigh, North Carolina 27695-7908
(Received 26 August 1998; revised manuscript received 21 December 1998)

Shock compression of polycrystalline copper was numerically investigated by use of a discrete-element model to highlight underlying heterogeneous and nonequilibrium processes at the grain level. The average diameter of model grains was 12 μm. Results show highly transient vortical flow fields and strong particle velocity dispersion that are consistent with the experimental results of Mescheryakov and his associates. Characteristic times for these phenomena were on the order of acoustic propagation times across the grains. The number of vortices increased with shock strength, but their size decreased almost inversely. Ejection of copper particles from the back free surface of the specimen was also observed. The cause of ejection is grain boundary cracking. [S0163-1829(99)06421-8]

I. INTRODUCTION

For almost a decade now, Meshcheryakov and his associates have been investigating the shock response of metals at the grain level by use of a two-channel interferometer and optical and electron microscopy.[1–4] Among many features they discovered at the grain level (details of the experiment are given in Sec. III), there are several key observations that are relevant to the present investigation. They are (1) a nonequilibrium distribution of shock-induced particle velocity, (2) particle velocity dispersion (defined as the standard deviation of particle velocity distribution at the grain level), (3) a rotational mode of deformation that is said to be caused by the particle velocity dispersion, and (4) dynamic fracture mechanisms that are controlled by the rotational deformation. It was also speculated that ''turbulent-like microflows may occur in polycrystals when the particle velocity dispersion reaches a certain critical level.'' [5]

The concept of the rotational deformation described above was first proposed by Panin and his associates as a distinct carrier of solid deformation at the grain level (described as meso or structural levels).[6] They indicated that conventional mechanisms of crystallographic shear are of translational nature and inadequate to describe completely the plastic deformation of solids that have unique hierarchical microstructures and interior boundary surfaces. The translational mode of deformation is said to be incapable of fully reflecting ''the nature of dislocation sources and the relationship governing the self-organization of dislocation ensembles'' at the structural level. To better describe the plasticity of solids at the structural level, they introduced the concept of ''structural deformation elements (volume).'' The motion of such a finite sized structural element involves both translation and rotation. The subject was recently reviewed by Panin.[7]

Among many theoretical investigations of the above described idea, in Russia, the work of Makarov contains the most extensive model calculations[8,9] which attest to the importance of rotational deformation and vortical velocity fields at the grain level. His model is an interpretation of Panin's concept, through use of the Cosserat theory[10] in which every point of the continuum consists of a small rigid body. Thus, the deformation of this continuum is described not only by the displacement, but also by the rotation of the rigid element, both depending on position and time. The governing equations of Makarov (see Sec. II) are identical in form to those found in micropolar elasticity.[10]

The well-acknowledged difficulty in dealing with the micropolar equations is the determination of constitutive equations concerning the couple stress and the nonsymmetric component of the stress tensor. At present there is no known experimental technique to determine these properties unambiguously. In early calculations,[8] Makarov used *ad hoc* assumptions to determine the materials constants. No specific value was mentioned for the couple stress constants. In a more recent calculation,[9] he avoided use of the couple stress. The rotational motion is controlled only by the nonsymmetric stress which is postulated to be a linear function of the second invariant of total plastic strain to imitate the behavior of single crystals. No explanation for the choice of the constant was given.

Meyers and Carvalho investigated the dispersion of shock wave propagation in polycrystalline solids using a probabilistic model of crystal orientation.[11] They found that the wave front becomes irregular as it propagates into the material. For instance, for a planar shock wave in nickel whose grain size is 10 μm, the irregularity becomes 16 μm thick when the wave has propagated 1.5 mm into the material. Since the thickness of the irregularity is comparable to the grain size, it was concluded that ''the grains are subject to a stress state that is obviously different from the one that would be imposed by a perfectly planar wave.''

In all, there is strong evidence, both experimental and analytical, that indicates the existence of heterogeneous, nonequilibrium processes in shock compression of metals at the grain level that are not described by the orthodox continuum model of shock wave structure.[12] In this study, we investigated the shock response of polycrystalline copper at the grain level through use of a discrete-element code called DM2. This code, described in Sec. II, was developed at North Carolina State University in collaboration with S. Psakhie of the Russian Materials Center, Tomsk. Section III

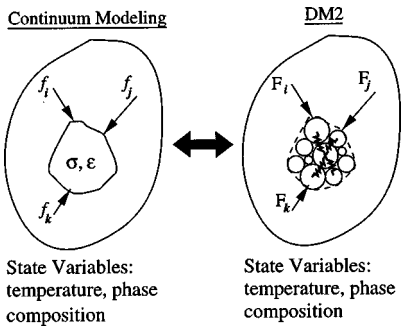

FIG. 1. Schematic illustration of discrete element modeling in comparison with continuum modeling.

discusses the computational model of polycrystalline copper. Results are presented in Sec. IV.

II. DM2 CODE

The fundamental theory and basic capabilities of the DM2 code are described in Ref. 13. What follows is a recapitulation of those elements that are directly relevant to the present calculation for purpose of a self-contained discussion. The DM2 code is a two dimensional, quasimolecular dynamics code in which material bodies are represented by single particles (called elements) and/or by an assembly of such elements. Figure 1 illustrates a schematic of the basic idea. A space occupied by materials is divided into a finite number of interacting discrete elements. In many of the applications we have considered,[13–15] the elements had diameters on the order of micrometers. But in special applications these elements may have much larger dimensions depending on the relative scale of microstructure with respect to the overall dimension of the system under consideration.[16,17]

Although materials mass is represented by ''discrete elements'' in the DM2, the underlying methodology is still a continuum modeling of materials behavior. It assumes that thermomechanical response can be effectively represented by the aggregate motion of interconnected discrete elements and the evolution of their internal state parameters such as temperature and composition. For example, Fig. 2 is a schematic illustration of fracture and plastic deformation in the DM2 representation. Obviously, plastic deformation involves both translation and rotation of elements. But, an important departure from the usual continuum modeling is that the motion of elements is governed by classical dynamics (quasimolecular) and not circumscribed by the form of continuum conservation equations. Nevertheless, the DM2 does not violate the conservation of mass, momentum, and energy.

There are several advantages of the DM2 over orthodox continuum approaches. For example, microstructural geometry that contains inhomogeneity and anisotropy can be easily developed by the selective assignment of material properties, bonding and contact states of elements, and areas of materials discontinuities. Interfacial layers and properties can be treated in a simple, realistic fashion. These properties can also be selectively distributed among elements and clusters of elements. The difficult problem of dealing with mass penetration and mixing in continuum description does not require any special consideration.

The mechanical interactions between two elements in the

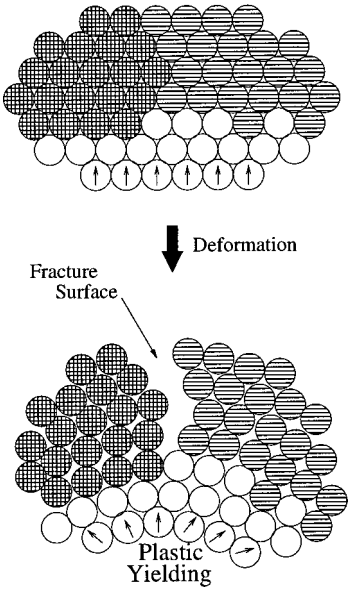

FIG. 2. Schematic illustration of fracture and plastic deformation in discrete element representation. Particles of different shading represent deferent materials. Arrows show rotation of particles during plastic deformation.

current code are schematically illustrated in Fig. 3(a). The total interaction force between a pair of elements consists of a force from the central potential, a shear force, a central damping force, a tangential damping force, and a dry friction force. These forces are regarded as effective, discrete-element representations of materials response behavior. In the DM2, stress at a point is defined at the center of an element using forces acting on its surface. Momentum balance is considered for one side of an element separated by a cross section at element centroid,

$$A\sigma_{ij}n_i=\sum_{k=1}^{l'} f_j^k-\frac{M}{2}a_j\,, \tag{1}$$

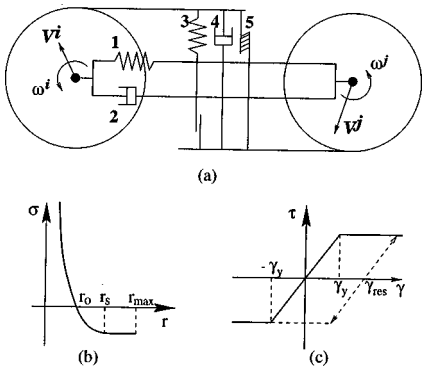

FIG. 3. Schematic illustration of mechanical interaction models in DM2. Interaction forces are (1) central potential force, (2) central damping force, (3) shear resistance force, (4) tangential damping force, and (5) dry friction force. Model parameters are r_s (interelement distance at yielding), $r_{\max}$ (interelement distance at braking of the bond), γ_y (yielding shear strain), and $\gamma_{\rm res}$ (residual shear strain). Superscripts i and j represent elements i and j, **v** is the translational velocity, and $\boldsymbol{\omega}$ is the angular velocity.

where subscripts i and j signify indices of coordinates, A is the cross section area, n_i is the normal vector pointing outward, σ_{ij} is the stress tensor, f_j^k is the interaction force of element k ($k=1,...,l'$) and M is the element mass. The acceleration of the element a_j is defined as follows:

$$a_j=\sum_{k=1}^{l}\frac{f_j^k}{M}, \tag{2}$$

where l is the total number of interacting elements.

Strain is harder to define than stress and typically involves the positions of contacting neighbor elements. Since the neighborhood changes during motion, only Eulerian strain ϵ_{ij} is defined. For a pair of elements m and k,

$$\Delta\epsilon_{ij}^{mk}=\frac{1}{2}\left(\frac{\Delta u_i^{mk}}{L^{mk}}n_j^{mk}+\frac{\Delta u_j^{mk}}{L^{mk}}n_i^{mk}\right), \tag{3}$$

where L^{mk} is the distance between two element centers, n_i^{mk} is the component of a unit vector in the radial direction originated at the center of element m. $\Delta\epsilon_{ij}^{mk}$ and Δu_i^{mk} are increments of strain and relative displacement at the contact point between the elements. The shear components of the strain reflect the displacement in the transverse direction. Equation (3) may be averaged over all interacting elements to evaluate the strain increment at the element centroid, $\Delta\epsilon_{ij}^{m}$.

$$\Delta\epsilon_{ij}^{m}=\sum_{k=1}^{l}\frac{\Delta\epsilon_{ij}^{mk}}{l}. \tag{4}$$

The central interaction potential can be represented by a variety of functions, but the Lennard-Jones potential was used in the present calculation. The resulting central potential force between element i and j, $\mathbf{f}_P^{ij}$, is

$$\mathbf{f}_P^{ij}(r)=-\frac{\alpha mn}{r_0(n-m)}\left\{\left(\frac{r}{r_0}\right)^{-(n+1)}-\left(\frac{r}{r_0}\right)^{-(m+1)}\right\}\mathbf{n}^{ij}, \tag{5}$$

where r is the interelement distance, r_0 is the equilibrium value of r. α, m, and n are the material parameters that represent effective hydrostatic compression behavior ($n>m$). $\mathbf{n}^{ij}$ is the unit vector in the radial direction pointing from element i to j. In the present calculation, the Hugoniot data were used to determine these coefficients. In tension, the above function is supplemented by a temperature dependent yielding segment as shown in Fig. 3(b). The shear resistance is described by an elastic, perfectly plastic model as illustrated in Fig. 3(c). The dry friction is based on Coulomb's law of friction. The central damping force is assumed to be a linear function of the radial relative velocity.

$$\mathbf{f}_D^{ij}=C_n\mathbf{v}_n^{ij},$$

$$\mathbf{v}_n^{ij}=(\mathbf{v}_s^{ij}\cdot\mathbf{n}^{ij})\mathbf{n}^{ij},$$

$$\mathbf{v}_s^{ij}=\mathbf{v}^j-\mathbf{v}^i-(q^{ji}\boldsymbol{\omega}^j+q^{ij}\boldsymbol{\omega}^i)\times\mathbf{n}^{ij}, \tag{6}$$

where $\mathbf{f}_D^{ij}$ is the damping force acting on element i due to element j, $\mathbf{v}_n^{ij}$ is the relative radial velocity of element j with respect to i, $\mathbf{v}_s^{ij}$ is the relative velocity of element j with respect to i at the contacting point, C_n is the damping coefficient, $\mathbf{v}^i$ and $\mathbf{v}^j$ are translational velocities of elements i and j, $\boldsymbol{\omega}^i$ and $\boldsymbol{\omega}^j$ are the angular velocities of elements i and j, q^{ij} is the distance between the contacting point and the center of element i, and q^{ji} is the distance between the contacting point and the center of element j.

TABLE I. Bonding states between elements.

$r\leqslant r_{\min}$[a]	Linked and in contact
$r_{\min}<r\leqslant r_0$	Linked and in contact if the elements were linked previously, or in contact otherwise
$r_0<r\leqslant r_{\max}$[b]	Linked if the elements were linked previously, or unlinked and not in contact otherwise
$r_{\max}<r$	Unlinked and not in contact

[a] $r_{\min}$: Minimum interelement distance below which unlinked elements become linked.

[b] $r_{\max}$: Maximum interelement distance beyond which linked elements become unlinked.

Damping forces are used to represent inelastic collision of elements as well as to control high frequency oscillations. A quadratic function was also tested, but did not reveal any new feature. In applications we have considered so far, the radial interactions were sufficient for the hydrodynamic description of solids under high-pressure shock wave compression.

The connectivity between a pair of neighboring elements in the DM2 code is a function of the relative central distance. Bonding states are summarized in Table I. Depending on the connectivity status, different interaction forces are selectively activated. For example, frictional force is used only for the element pairs that are in contact, but which are not linked (no bond). Also, these mechanical states can be manipulated to create heterogeneous, initial microstructures such as flaws, cracks, and weakly bonded interfacial regions.

The motion of elements is described by classical dynamics. The governing equations for element i, having mass M^i and inertial moment J^i are given by

$$M^i\ddot{\mathbf{r}}^i=\sum_{j=1}^{l}\mathbf{F}^j, \tag{7}$$

$$J^i\ddot{\boldsymbol{\Theta}}^i=\sum_{j=1}^{l}\mathbf{K}^j, \tag{8}$$

where double overdots (¨) signify second order time derivative, $\mathbf{r}^i$ and $\boldsymbol{\Theta}^i$ are position and angular vectors of element, $\mathbf{F}^j$ and $\mathbf{K}^j$ are the force and moment due to interacting neighbors, and l is the number of interacting elements. These equations are comparable to the micropolar elasticity[10] used by Makarov in which the equations of motion have the form

$$\rho\ddot{u}_i=\sigma_{ij,j}, \tag{9}$$

$$J_i\ddot{\theta}_i=\epsilon_{ijk}\sigma_{jk}+\mu_{ji,j}, \tag{10}$$

where the first equation is the ordinary equation of motion in continuum mechanics except the nonsymmetric stress tensor σ_{ij}, J_i is a measure of the rotational inertia, θ_i is the rotation angle, ϵ_{ijk} is the alternator tensor, and μ_{ij} is the couple (or moment) stress required by the assumption that moment as well as force is transmitted through an area separating two

parts of a body. The closure of Eqs. (9) and (10) requires the constitutive equations for nonsymmetric σ_{ij} and μ_{ij}. The latter involves a torsion rate tensor. The inclusion of inelastic deformations can be dealt with formally by separating the force and couple stresses into elastic and inelastic parts.[8] But, very little specifics are given in Ref. 8. In a more recent paper,[9] the driving force for rotation is specified by the antisymmetric components of the stress tensor,

$$\sigma_{ij}^{A} = -\sigma_{ij}^{A} = \beta F[\mathrm{grad}(\epsilon^{p})], \tag{11}$$

where β is a material parameter, F is a fitting function, and ϵ^{p} is plastic strain.

The micropolar theory is a mathematically consistent extension of continuum theory to include rotation for structural elements of deformations at the mesolevel. But it has the disadvantage of introducing greater conceptual cost, complexity, and constitutive equations that are near impossible to determine experimentally at the present time. In contrast, the DM2 formulation is physically motivated and does not require any new ideas such as the asymmetric stress and the couple stress. One *ad hoc* feature, however, is the use of effective interaction forces that are not intuitively evident except for materials such as powders and granules.

In solving the dynamic equations, the DM2 imposes two conditions on time increment. They are (1) that elements cannot penetrate each other along the radial line in one time step and (2) that the momentum transferred between two elements in a single time step should not exceed the total momentum exchange during the whole collision process. The latter is equivalent to the Courant stability condition for numerical solution of hydrodynamic conservation equations. The equations of motion are integrated by use of a second order leapfrog method.

The DM2 contains several internal variables such as temperature, composition, and thermodynamic potentials to deal with thermochemical processes. At the grain level on the order of micrometers, dynamic loading creates a highly nonuniform temperature field and heat conduction can no longer be considered a slow process. In the current code, the temperature change of an element consists of two mechanisms. The first is the dissipation of mechanical energy given by

$$\Delta T^{i} = \frac{de^{i}}{C_{v}^{i} M^{i}}, \tag{12}$$

where ΔT^{i} is the temperature change over one time interval, de^{i} is the total increment of dissipated energy, C_{v}^{i} the specific heat at constant volume, and M^{i} the mass of element i. The above expression assumes implicitly that the interaction potentials are isentropic functions. That is, the effect of isentropic compression on radial force is subsumed in the potential function. The second mechanism is heat conduction, which is treated by Fourier's law where heat flux is proportional to the gradient of temperature between two linked or contacting elements:

$$\Delta Q = -\lambda \frac{T^{i} - T^{j}}{d} A \Delta t, \tag{13}$$

where ΔQ is the heat transfer from element j to i over one time step Δt, λ is the thermal conductivity, T^{i} and T^{j} are the temperatures of element i and j, and d is the interelement distance.

Regarding the thermal effects, we note that simulation of shock wave propagation in a linear chain using the viscous damping and the temperature changes described above shows that the overall temperature change between initial and terminal states is independent of the damping coefficient and that the magnitude agrees with that expected from the jump conditions. The viscous damping affects only the shock rise time. Thus, the conservation of energy is not influenced by the choice of damping coefficient.

III. DM2 SIMULATION OF THE MESCHERYAKOV EXPERIMENT

The Meshcheryakov experiment that motivated our investigations is a plane impact testing of metallic plates with a 37 mm bore diameter compressed air gun. Impacting and target plates are made of the same material. The range of impact velocity was 50–500 m/s. In the majority of tests the thickness of the plates (3–10 mm) was adjusted to produce spalling in the target plate. Free surface velocities of targets were monitored by a two-channel interferometer with 90° phase shift between interference signals. The beam was focused to an area having the diameter of 80–100 μm and detects particle motion, called mesoparticle velocity, over an area of 5–10 μm in diameter. The combination of the signals with 90° phase shift provides the mesoparticle velocity dispersion (PVD), which is defined as the width of the particle velocity distribution over the laser beam cross section (see Ref. 18 for mathematical details). Interferometers used elsewhere (for example, VISAR) suppress the distribution to improve the measurement of average velocity.

The measurement of PVD, in conjunction with metallurgical observations of post shock samples by optical and electron microscopy, was used to gain insight into the mesomechanical features of plastic and fracture behavior of metallic materials that are subjected to high pressure shock wave compression. The materials studied include copper, ductile steel, aluminum, aluminum alloys, and titanium. Copper was chosen for our study because of its low shear strength.

Some early calculations of the Mescheryakov experiment were reported in Ref. 19 where a formation of vortical velocity fields and particle velocity dispersion were observed in a region immediately behind the shock front for a relatively low velocity (89 m/s) impact. In the present study, computational impact tests were performed for two impact velocities: 89 m/s and 250 m/s. At present there is no experimental data for the high velocity impact. Also, a new computational copper specimen, which has a better back free surface profile than that of the previous specimen, was developed.

The new model specimen was created by a slow compression of copper particles of 12 μm in diameter, on the average. The particles in the starting specimen become grains in the final specimen. Element diameter was 1 μm. The orientation of element packing in each particle was assigned randomly to create local anisotropy. Voids between particles were eliminated by compression of particles. When elements

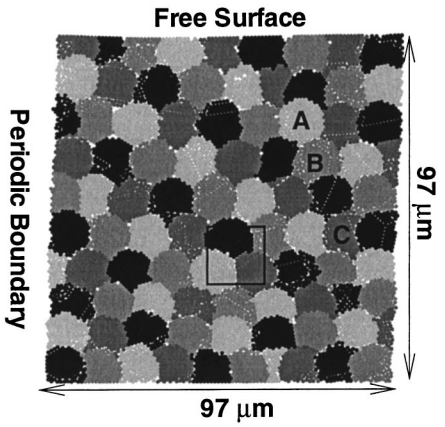

FIG. 4. Initial geometry of the model copper specimen. The rectangle about the center and grains *A*, *B*, and *C* are referenced in Fig. 5 and Fig. 11, respectively.

of neighboring particles come into contact, they form bonds with grain boundary strength. After compression to the terminal density of 95% TMD (theoretical maximum density), the applied load was gradually reduced to zero. This percentage is arrived at by using the formula, n_{elm}/N where n_{elm} is the number of elements in the specimen and N is the number of elements if the specimen were filled in a dense-packing arrangement. Maximum local residual stress of ± 0.05 GPa was found in some of grain boundary elements. The residual stress is considered negligible when compared with the shock pressure of 3 to 10 GPa in this study.

The initial geometry of the model specimen is shown in Fig. 4 where individual grains have, on the average, about 113 elements. We consider this number to be the minimum required for evaluating the velocity and stress distributions within a single grain. The diameters of these grains were chosen to be comparable to the spatial resolution of the Mescheryakov's interferometer. The region marked by a rectangle in Fig. 4 is enlarged in Fig. 5 to illustrate a triple point grain boundary and anisotropy of grain orientations.

To reduce computing time, the model specimen was arranged to impact a rigid wall located at bottom of the specimen. Thus, the initial velocity of the specimen is half of the impact velocity in Meshcheryakov experiments. That is, the velocity of 89 m/s is equivalent to the impact test of 178 m/s

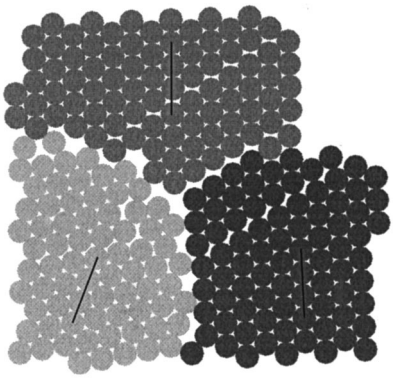

FIG. 5. An enlarged triple point grain boundary in the region marked by a rectangle in Fig. 4. Line segments in individual grains are drawn to show the anisotropy of grain orientations.

(Ref. 2). The velocity of 250 m/s was chosen to represent the upper limit of their velocity range. To eliminate transverse boundary effects, the left and right boundaries were made periodic.

The model material was assumed to have no shear strength. So, only the central potential and central damping forces were activated for mechanical interactions. The magnitude of the latter f_D is given by

$$f_D = C_n \Delta u, \tag{14}$$

where C_n and Δu are the damping coefficient and relative velocity of an element pair in the radial direction, respectively. At present there is no mesomechanical model to evaluate C_n for shock loading. Therefore, in the present investigation, we evaluated this coefficient by assuming that the stress due to the central damping force is equivalent to shear yielding viscous stress τ_s proposed by Band[20] and others[21,22] to describe global energy dissipation processes in shock compression of solids. In one spatial dimension τ_s is given by

$$\tau_s = \eta \dot{\epsilon} = \eta \frac{du}{dx}, \tag{15}$$

where η is effective viscosity, u is the particle velocity, and x is the spatial coordinate taken in the direction of the wave propagation. By the assumption,

$$\frac{C_n \Delta u}{A} = \eta \frac{du}{dx}, \tag{16}$$

where A is the cross section area between elements. By considering a unit length in the direction perpendicular to the coordinate axes, the cross sectional area in two spatial dimensions is $A = d \times 1$, where d is the diameter of an element. The velocity gradient in the right-hand side over the distance of d is Δu to the first order. So, Eq. (16) yields

$$C_n \approx \eta. \tag{17}$$

The value of η is taken from the work of Grady[21] in which the viscosity is defined as the ratio of the maximum shear difference between the Rayleigh line and the Hugoniot hydrostat and the average strain rate associated with the compressive shock. In this model, η becomes a function of shock pressure p_h given by

$$\eta = k p_h^{-2}, \tag{18}$$

where k is the material constant. For copper, k is determined to be 271.4 $(\mathrm{GPa})^2\,\mathrm{Pa\,s}$.[22] Hydrocode application of this model in a three-dimensional framework shows that this constant reproduces well the measured wave profiles of copper, for the pressure range of our interest.[22] Other material parameters used in the calculation are listed in Table II.

IV. RESULTS AND DISCUSSIONS

The calculated steady stress behind the shock front was lower than that expected from the jump conditions. For example, the shock pressure for the impact velocity of 250 m/s was 8.0 GPa, whereas the corresponding magnitude by the jump conditions is 9.6 GPa. The reduction in two dimensions

TABLE II. Material parameters used in the discrete element calculation.

α (mJ)	m	n	C_n (kg/s)	r_{max}/r_0	r_{min}/r_0
0.697	1	2	25.7,[a] 2.91[b]	1.01[c]	0.90[d]

[a,b]For 89 m/s and 250 m/s impact velocities, respectively.
[c]Based on spall stress of copper (Ref. 23).
[d]Selected so that initially unlinked pair will never be linked.

is attributed to the following two effects: (i) the existence of about 5% void space and (ii) a reduction in effective longitudinal wave propagation speed due to random orientation of grains. In the current calculation, the interaction coefficients were determined so that the shock speed agrees with the jump conditions when grain orientations are aligned in the direction of wave propagation. Thus, when the grains are randomly oriented, the longitudinal speed decreases accordingly. This shows that an appropriate distribution of the interaction coefficients must be considered in order to improve the calculation of shock speeds in polycrystals.

Figure 6 shows the velocity field at 14 ns after impact, with an impact velocity of 89 m/s. It is clearly evident that the wave front is nonuniform and located somewhere between 35 to 45 μm from the impact end. Also, we observed the appearance of a flow field with localized rotational deformation. The vortical structure is highly transient and depends greatly on such parameters as shock strength and local microstructure. The typical lifetime of these vortices is on the order of a few nanoseconds that are comparable to acoustic propagation times across the grains.

As indicated in the Introduction, there exists a parallel between DM2 and Makarov's approach. But the origins of the rotational velocity field are not exactly identical. In the former, vortices are caused by the interaction of shock-induced flow with both local anisotropy and grain boundaries. There is no explicit dependency on plastic strain. It results from complex interplay between flow and grains. But,

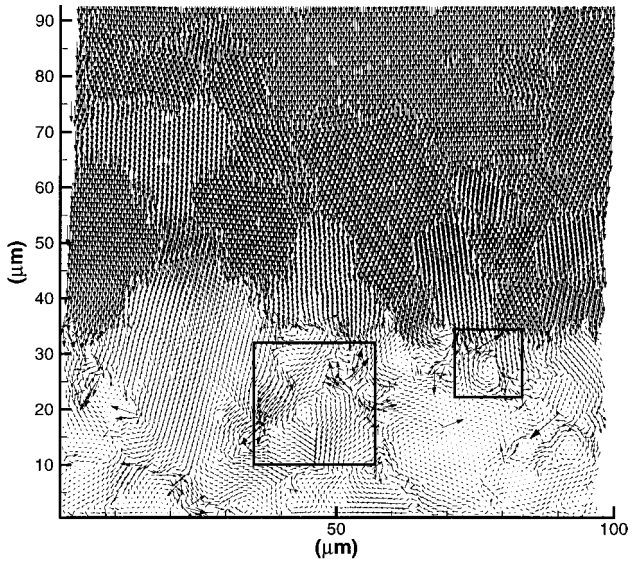

FIG. 6. Velocity field in the model specimen at 14 ns after impact for the 89 m/s simulation. The two rectangles are explained in Figs. 7(a) and 7(b).

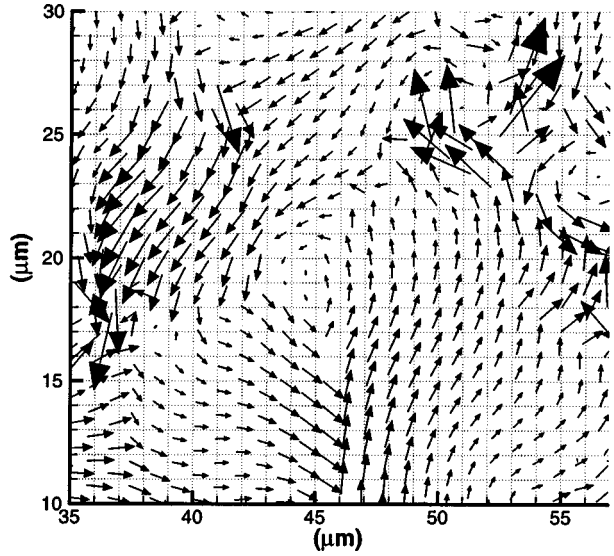

(a)

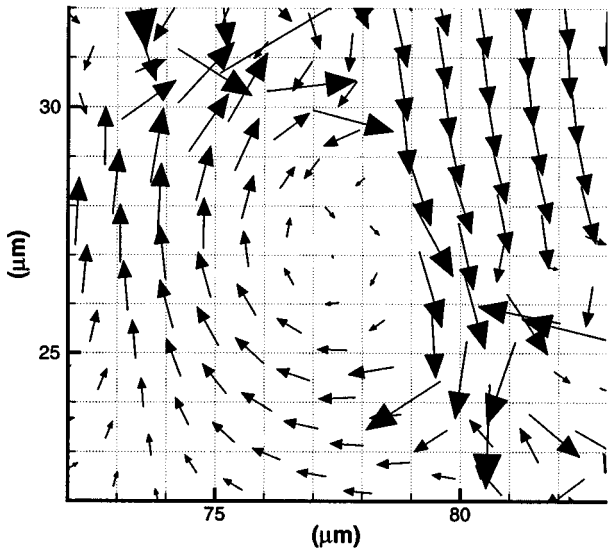

(b)

FIG. 7. An enlarged view of the velocity field marked by (a) the large and (b) the small rectangles in Fig. 6.

in the latter, the key factor is the postulated asymmetric stress as a function of plastic strain that tends to localize in the region of stress concentration, such as grain boundary. So, the rotation of mesovolumes that arises from localized strain is built into the model with some difficult-to-determine parameters.

Two major vortices in Fig. 6 are marked out by rectangular borders and are magnified in Figs. 7(a) and 7(b). The size of these structures is in the range of 10 to 15 μm. The region of the vortex of Fig. 7(a) lies within a single grain, but the one in Fig. 7(b) is found at a triple point grain boundary. No preferred locations were observed for the formation of localized vortical flow.

The vortex in Fig. 7(b) has a diameter of about 10 μm and the circumferential velocity of 50 m/s. So, the rotational shear rate of the vortex is on the order of 10^7 l/s. According to Mescheryakov, such an intense localized velocity field,

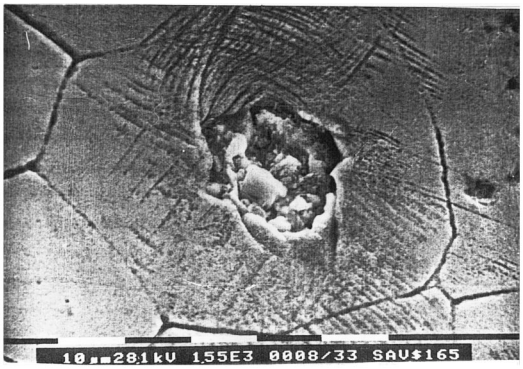

FIG. 8. Fracture pattern observed in the experiment by Mescheryakov and his associates. The fiducial lines represent 10 μm. (Courtesy of Yu. I. Mescheryakov.)

coupled with the existing microstructure, results in the rotational mode of deformation which, at appropriate conditions, lead to fracture and shear banding.[1] One such example is shown in Fig. 8. In our calculations, however, we have not observed fracturing of grains in the interior of the specimen while it was in compression.

Flow fields for the impact velocity of 250 m/s were quite different from those of the low impact velocity. Small vortices shown in Fig. 9, having the diameter less than 5 μm, became ubiquitous. Overall velocity fields appeared disordered. The decrease in dimensions of vorticity is almost inversely proportional to the impact velocity. That is, there is a three-fold decrease in diameter for the velocity change of 89 to 250 m/s. A similar observation was made in a recent, molecular-dynamics study of structure formation in single crystals under high-pressure shock wave compression.[24] Both results suggest the existence of a general rule between the scale of shock-induced microstructures and shock strength. At present, there is no theoretical model for such a relationship at the mesolevel.

Mescheryakov suggested that the ratio of particle velocity

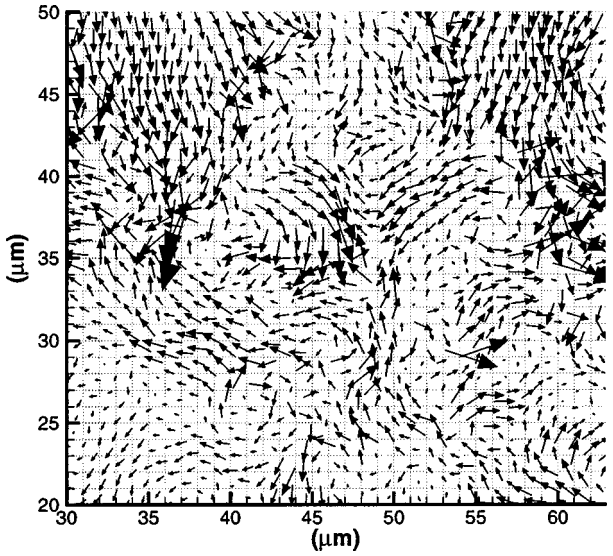

FIG. 9. Eddy-like velocity fields are observed immediately behind the shock front for the 250 m/s simulation at 18 ns after impact.

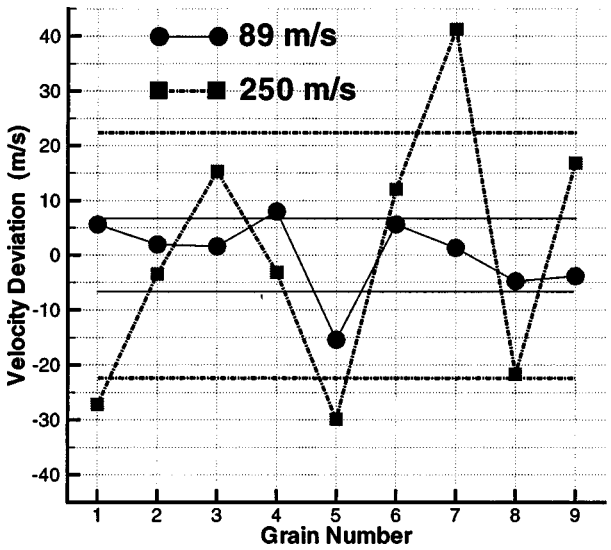

FIG. 10. Particle velocity deviation from the average for individual grains at the back free surface.

dispersion Δu_p, to the average particle velocity, u_p, is an indicator of the transition to the rotational mode of deformation. In the present computation, however, the ratios for the two cases were found to be about the same as discussed below. Thus, for the two cases that were investigated, the ratio $\Delta u_p/u_p$ is not a sensitive parameter to differentiate the flow patterns.

In Mescheryakov's experiment, PVD, which was measured at the back free surface, $\Delta u_p^{\mathrm{FS}}(=2\Delta u_p)$, was the largest at the median point of the rising shock front. This value was 14 m/s for the 178 m/s symmetric impact test. This velocity corresponds to 89 m/s in the numerical simulation, where the particle velocity dispersions were evaluated when the average back free surface velocity reached half of the impact velocity. Timewise, the maximum dispersion occurred at approximately 40.8 ns and 33.5 ns after impact for 89 m/s and 250 m/s, respectively. Since the measurements are said to have a spatial resolution of 3 to 5 μm, the computational free surface velocities are also averaged over a similar distance. That is, the velocities are averaged over grains that are located at the free surface. The results are shown in Fig. 10. In this figure, the particle velocity deviation from the average is shown for each grain. Two pairs of parallel lines represent the standard deviations of granular particle velocity from the average for the two impact velocities. For the 89 m/s case, the width of the particle velocity distribution is 13.5 m/s, which agrees well with the measured value of 14 m/s. The dispersion for 250 m/s is 44.6 m/s. There is no experimental value yet for this velocity.

The ratio of particle velocity dispersion to impact velocity at the median point, $\Delta u_p/u_p$, is about the same for the two cases investigated: $6.75/89 \approx 0.076$ and $22.3/250 \approx 0.089$. An additional calculation for the impact velocity of 175 m/s gave the value of $\Delta u_p/u_p$ to be $14.5/175 \approx 0.083$. Comparable experimental data for steel is $12.4/139 \approx 0.089$ (Ref. 3). Therefore, there may be a weak dependence of Δu_p on u_p, but at present, we do not find it to be a sensitive indicator of flow characteristics.

Reynolds number at the grain level is also of interest,

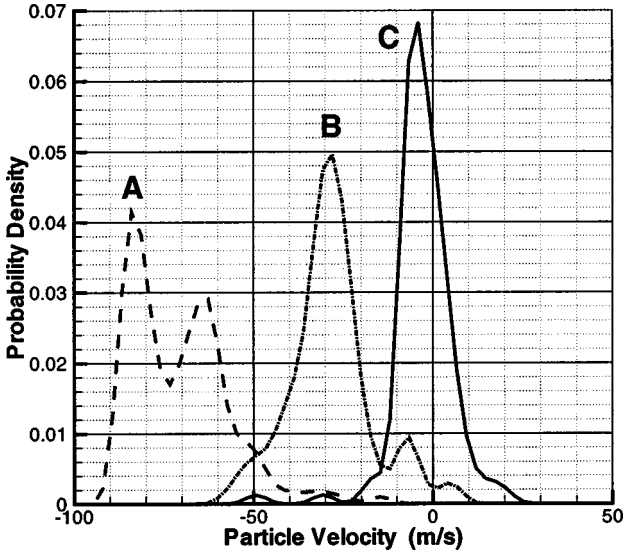

FIG. 11. Profiles of the particle velocity distribution function within three grains indicated by *A*, *B*, and *C* in Fig. 4 for the 89 m/s simulation.

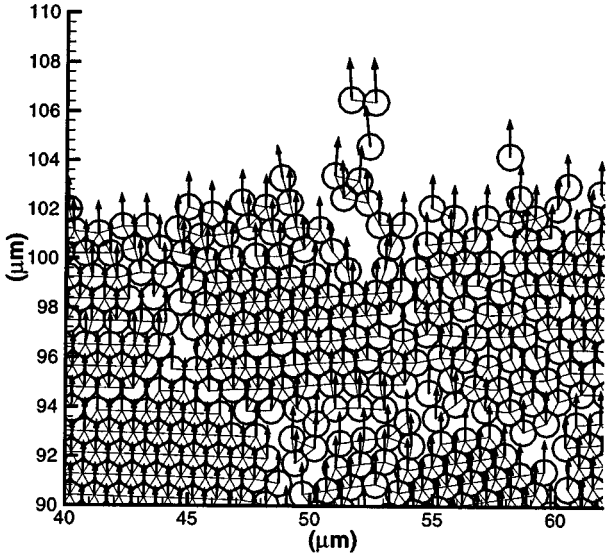

FIG. 12. Ejection of elements from the back free surface with velocity vectors and element links for the 250 m/s simulation.

particularly the value associated with the fluctuating flow, Δu_p:

$$Re = \frac{\rho D \Delta u_p}{\eta}, \tag{19}$$

where ρ is the local density and D is the grain diameter (12 μm on the average). For the impact velocity of 250 m/s where the flow was characterized as ''unstable state'' by Mescheryakov, $\rho = 9.48\ \mathrm{g/cm^3}$ and $\eta = 29\ \mathrm{dyn\ s/cm^2}$. Thus, the Reynolds number for the local flow is $Re = 0.87$. Surprisingly, this number is close to the value of unity Mescheryakov hypothesized to describe the flow regime. Using a fluid dynamic analogy, he suggested that 'the energy exchange between adjacent flows that are separated by zones of vortex motion is negligibly small and the ''turbulence'' becomes independent of external conditions.' [2] In contrast, for the impact velocity of 89 m/s, $\rho = 9.13\ \mathrm{g/cm^3}$ and $\eta = 252\ \mathrm{dyn\ s/cm^2}$. These values yield $Re = 0.029$, which is only 1/30 of the number for 250 m/s. Therefore, for the 89 m/s case, the inertia force is much smaller than the viscous force at the grain level. This is consistent with the observation that small scale vortices were absent in the 89 m/s impact calculation.

Another result of interest is the distribution of particle velocity itself. It will shed light on the nonequilibrium nature of shock compression in macroscopically homogeneous, polycrystalline metals. Figure 11 shows the distribution functions of longitudinal particle velocity for the case of 89 m/s at three different locations identified as *A*, *B*, and *C* in Fig. 4. These locations represent three distinct points: within the rising shock front, immediately behind it, and a certain distance away from the front. The distribution evolves from a Poisson-type distribution to a more normal Maxwellian distribution, indicating that nonequilibrium effects are the hallmark of the shock compression process at the grain level. If the location of grain *C* is used to estimate the characteristic relaxation time τ for the distribution, then τ can be estimated by l/U_s where l is the longitudinal distance between the centers of grain *A* and *C*. The value estimated is 11.5 ns. This magnitude is comparable to several times the sound wave propagation across the grains.

The appearance of multipeaks in the distribution functions reflects the fact that the direction and magnitude of particle velocities have some features over the dimension of a single grain. But, the exact causes are not yet well understood. The nature of multipeaks may be affected by factors such as grain size, element size, and lattice anisotropy.

Finally, we have observed the ejection of copper elements from grain boundaries at the free surface. Such ejection is reported in Ref. 25. Figure 12 shows an example of ejecting elements from the free surface for the impact velocity of 250 m/s. There was no ejection of elements for 89 m/s. Linked elements are connected by solid lines. The key factor that controls the ejection is cracking along grain boundaries in the horizontal direction, again emphasizing the nonplanarity of ''plane wave loading'' at the grain level. Interestingly, the velocity vectors of ejecting elements are almost parallel to the direction of wave propagation, and the ejection velocities were about 1.3 times larger than the average free surface velocity. However, no attempt is made to compare the results with experimental data because of the preliminary nature of the calculation.

V. CONCLUSION

Shock wave loading of polycrystalline copper was numerically investigated by means of a discrete-element model. Nonuniform wave front and complex flow patterns were observed and are attributed to anisotropy in crystal orientation and grain boundary surfaces in the polycrystal. Formation of vortical flow was observed for the impact velocity of 89 m/s.

The average dimension of vortices was 10–15 μm. The corresponding local strain rate was on the order of 10^7 l/s. The calculated particle velocity dispersion at the back free surface was 13.5 m/s, which is in agreement with the experimental value of 14 m/s. For the impact velocity of 250 m/s, the average dimension of vortices decreased to about 5 μm. Vortices became ubiquitous and the overall flow field appeared to be disordered.

ACKNOWLEDGMENT

The present research is partially supported by U.S. Army Research Office (Grant No. DAAH 04-94-G-0033). [The authors express special thanks to the reviewer who brought our attention to the scaling relationship discussed in Ref. 24 and recommended an extended description of DM2 and works of Makarov and Mescheryakov.]

[1] Yu. I. Mescheryakov and A. K. Diavkov, Zh. Tekh. Fiz. **55**, 591 (1985) [Sov. Phys. Tech. Phys. **30**, 348 (1985)].
[2] Yu. I. Mescheryakov and S. A. Atroshenko, Izv. Vyssh. Uchebn. Zaved. Fiz. **4**, 105 (1992) [Russ. Phys. J. **35**, 385 (1992)].
[3] Yu. I. Mescheryakov, N. A. Mahutov, and S. A. Atroshenko, J. Mech. Phys. Solids **42**, 1435 (1994).
[4] M. G. Tomilin, Yu. I. Mescheryakov, S. A. Atroshenko, and N. I. Zhigacheva, Mol. Cryst. Liq. Cryst. Sci. Technol., Sect. A **251**, 343 (1994).
[5] G. G. Savenko, Yu. I. Mescheryakov, V. B. Vasil'kov, and A. I. Chernyshenko, Fiz. Goreniya Vzryva **26**, 97 (1990) [Combust. Explos. Shock Waves **26**, 585 (1990)].
[6] V. E. Panin, Yu. V. Grinyaev, T. F. Elsukova, and A. G. Ivanchin, Sov. Phys. J. **25**, 479 (1982).
[7] V. E. Panin, Physical Mesomechanics **1**, 5 (1998).
[8] P. V. Makarov, Russ. Phys. J. **35**, 334 (1992).
[9] P. V. Makarov, Physical Mesomechanics **1**, 57 (1998).
[10] W. Nowacki and W. Olszak, *Micropolar Elasticity* (Springer, Udine, 1974), No. 151.
[11] M. A. Meyers and M. S. Carvalho, Mater. Sci. Eng. **24**, 131 (1976).
[12] D. C. Wallace, Phys. Rev. B **22**, 1477 (1980).
[13] Z. P. Tang, Y. Horie, and S. G. Psakhie, in *High Pressure Shock Compression of Solids IV*, edited by L. Davidson, Y. Horie, and M. Shahinpoor (Springer, New York, 1997), p. 143.
[14] K. Yano and Y. Horie, J. Appl. Phys. **84**, 1292 (1998).
[15] S. Tamura and Y. Horie, J. Appl. Phys. **84**, 3574 (1998).
[16] O. J. Schwartz, Y. Horie, and M. Shearer, Phys. Rev. E **57**, 2053 (1998).
[17] S. G. Psakhie, Y. Horie, S. Yu. Korostelev, A. Yu. Smolin, A. I. Dmitriev, E. V. Shieko, and S. V. Alekseev, Russ. Phys. J. **38**, 1157 (1995).
[18] Yu. I. Mescheryakov and A. K. Divakov, DYMAT Journal **1**, 271 (1994).
[19] Y. Horie and K. Yano (unpublished).
[20] W. Band and G. E. Duvall, Am. J. Phys. **29**, 780 (1961).
[21] D. E. Grady, Appl. Phys. Lett. **38**, 825 (1981).
[22] J. W. Swegle and D. E. Grady, J. Appl. Phys. **58**, 692 (1985).
[23] D. J. Steinberg, Lawrence Livermore National Laboratory, Report No. UCRL-MA-106439, 1991 (unpublished).
[24] B. L. Holian and P. S. Lomdahl, Science **280**, 2085 (1998).
[25] C. Remiot, P. Chapron, and B. Demay, in *High-Pressure Science and Technology-1993*, edited by S. C. Schmidt, J. W. Shaner, G. A. Samara, and M. Ross (AIP, New York, 1994), p. 1763.